Supporting Information

Animal conflicts escalate in a warmer world

Science of The Total Environment

N. Fattorini[1], S. Lovari, S. Franceschi, G. Chiatante, C. Brunetti, C. Baruzzi, & F. Ferretti

Correspondence

[1]Niccolò Fattorini
Department of Life Sciences, University of Siena, Via P.A. Mattioli 4, 53100, Siena (Italy)
E-mail: niccolo.fattorini@unisi.it; niccolo.fattorini@gmail.com

Appendix 1. Analysis of the cumulative effects of weather on aggression rate

Table S1. Results of model selections conducted to investigate the cumulative effects of climatic conditions at different time windows (T: mean temperature; P: total amount of precipitation) on the *pro capite* aggression rate of chamois. The top-ranked, non-nested models within ΔAICc<2 are shown, with relevant K, AICc, ΔAICc and standardized weight. All models evaluated also included the chamois group identity as random intercept.

Time window length	Intercept	T	P	Site	Time	Time^2	Julian day	T × Site	P × Site	K	AICc	ΔAICc	Weight
15 days	X	X			X	X				7	1833.4	0.00	1
20 days	X	X			X	X	X			8	1836.2	0.00	0.553
	X	X			X	X				7	1836.6	0.04	0.447
25 days	X	X			X	X	X			8	1836.1	0.00	0.621
	X	X			X	X				7	1837.1	0.01	0.379
30 days	X	X			X	X	X			8	1837.6	0.00	0.475
	X	X			X	X				7	1838.4	0.08	0.314
	X				X	X				6	1839.2	1.60	0.211

Table S2. Parameters estimated from the best GLMM predicting the *pro capite* aggression rate of chamois at feeding, for each time window: variance of random intercepts (σ^2), predictors' coefficient estimates (β) and their 95% confidence intervals (CIs). An asterisk marks coefficients whose CIs do not include '0'. Effects of accumulated climatic conditions (mean temperature, T) on aggression rate are bolded. For measurement units of explanatory variables, and the best supported model at the 30 days-time window, see main text.

Time window length	**Random intercept**	**Predictor**	**β coefficient**	**95% CI**	
15 days	$\sigma^2_{GroupID} = 0.328$	Intercept	-3.296	-3.479; -3.113	*
		T_{15}	**0.254**	**0.078; 0.430**	*****
		Time of day	0.266	0.086; 0.446	*
		Time of day^2	0.181	0.026; 0.335	*
20 days	$\sigma^2_{GroupID} = 0.346$	Intercept	-3.296	-3.482; -3.110	*
		T_{20}	**0.264**	**0.067; 0.461**	*****
		Time of day	0.274	0.092; 0.456	*
		Time of day^2	0.179	0.025; 0.334	*
		Julian day	-0.162	-0.367; 0.043	
25 days	$\sigma^2_{GroupID} = 0.338$	Intercept	-3.298	-3.483; -3.113	*
		T_{25}	**0.275**	**0.071; 0.479**	*****
		Time of day	0.279	0.097; 0.461	*
		Time of day^2	0.181	0.026; 0.335	*
		Julian day	-0.185	-0.397; 0.027	

Appendix 2. Analysis of the cumulative effects of weather on aggression intensity

Table S3. Results of model selections conducted to investigate the cumulative effects of climatic conditions (T: mean temperature; P: total amount of precipitation) on the probability of chamois delivering a more aggressive behaviour pattern during feeding contests, at different time windows. The top-ranked, non-nested models within ΔAICc<2 are shown, with relevant K, AICc, ΔAICc and standardized weight. All models evaluated also included the chamois group identity as random intercept.

Time window length	Intercept	T	P	Site	Time	Time^2	Julian day	Opponent's relative age	Sender's age class	Contest type	T × Site	P × Site	K	AICc	ΔAICc	Weight
15 days	X		X				X	X		X			7	817.3	0	1
20 days	X		X				X	X		X			7	816.7	0	1
25 days	X		X				X	X		X			7	817.0	0	1
30 days	X		X				X	X		X			7	816.1	0	1

Table S4. Parameters estimated from the best GLMM predicting the probability of chamois delivering a more aggressive behaviour pattern during feeding contests, for each time window: variance of random intercepts (σ^2), predictors' coefficient estimates (β) and their 95% confidence intervals (CIs). An asterisk marks coefficients whose CIs do not include '0'. Effects of accumulated climatic conditions (total amount of precipitation, P) on aggression intensity are bolded. For measurement units of explanatory variables, and the best supported model at the 30 days-time window, see main text.

Time window length	**Random intercept**	**Predictor**	**β coefficient**	**95% CI**	
15 days	$\sigma^2_{GroupID}$ = 0.436	Intercept	2.202	1.807; 2.596	*
		P_{15}	**-0.314**	**-0.604; -0.025**	*****
		Julian day	0.551	0.249; 0.853	*
		Opponent's relative age (same)	0.489	0.035; 0.943	*
		Opponent's relative age (older)	-0.369	-0.913; 0.176	
		Contest type (escalated)	-0.827	-1.210; -0.445	*
20 days	$\sigma^2_{GroupID}$ = 0.407	Intercept	2.166	1.775; 2.557	*
		P_{20}	**-0.299**	**-0.551; -0.046**	*****
		Julian day	0.497	0.214; 0.779	*
		Opponent's relative age (same)	0.505	0.051; 0.959	*
		Opponent's relative age (older)	-0.367	-0.909; 0.175	
		Contest type (escalated)	-0.804	-1.187; -0.422	*
25 days	$\sigma^2_{GroupID}$ = 0.460	Intercept	2.162	1.764; 2.560	*
		P_{25}	**-0.282**	**-0.545; -0.020**	*****
		Julian day	0.460	0.172; 0.748	*
		Opponent's relative age (same)	0.507	0.051; 0.962	*
		Opponent's relative age (older)	-0.367	-0.912; 0.177	
		Contest type (escalated)	-0.798	-1.183; -0.413	*

Appendix 3. Analysis of the cumulative effects of weather on vegetation productivity

Table S5. Results of model selections conducted to investigate the cumulative effects of climatic conditions (T: mean temperature; P: total amount of precipitation) on the standardized EVI index, at different time windows. The top-ranked, non-nested models within ΔAICc<2 are shown, with relevant K, AICc, ΔAICc and standardized weight. All models evaluated also included the study year as random intercept and, following preliminary data exploration, had the dispersion modelled in relation to whether the daily EVI is interpolated and to the interaction T × Site.

Time window length	Intercept	T	P	Site	Julian day	T × Site	P × Site	K	AICc	ΔAICc	Weight
15 days	X	X	X	X	X		X	12	-910.8	0.00	1
20 days	X	X	X	X	X	X		12	-859.5	0.00	1
25 days	X	X	X	X	X	X		12	-820.8	0.00	1
30 days	X	X	X	X	X	X		11	-796.4	0.00	0.679
	X	X	X	X	X			10	-794.9	1.49	0.321

Table S6. Parameters estimated from the best GLMM predicting the standardized EVI index, for each time window: variance of random intercepts (σ^2), predictors' coefficient estimates (β) and their 95% confidence intervals (CIs). All models, following preliminary data exploration, had the dispersion modelled in relation to whether the daily EVI is interpolated and to the interaction T × Site (results of dispersion model not shown). An asterisk marks coefficients whose CIs do not include '0'. Effects of accumulated climatic conditions (mean temperature, T, and total amount of precipitation, P) on relative vegetation productivity are bolded. For measurement units of explanatory variables, see main text.

Time window length	**Random intercept**	**Predictor**	**β coefficient**	**95% CI**	
15 days	$\sigma^2_{Year} < 0.001$	Intercept	2.280	2.148; 2.412	*
		Julian day	-0.200	-0.244; -0.156	*
		T_{15}	**-0.111**	**-0.178; -0.044**	*****
		P_{15}	**0.183**	**0.057; 0.308**	*****
		P_{15} × Site (food-restricted)	**-0.148**	**-0.275; -0.021**	*****
		Site (food-restricted)	-0.372	-0.541; -0.203	*
20 days	$\sigma^2_{Year} = 0.048$	Intercept	2.301	1.964; 2.637	*
		Julian day	-0.189	-0.256; -0.121	*
		T_{20}	**-0.081**	**-0.263; 0.101**	
		P_{20}	**0.156**	**0.072; 0.239**	*****
		T_{20} × Site (food-restricted)	**-0.241**	**-0.427; -0.055**	*****
		Site (food-restricted)	-0.296	-0.472; -0.120	*
25 days	$\sigma^2_{Year} = 0.104$	Intercept	2.315	1.843; 2.787	*
		Julian day	-0.129	-0.206; -0.051	*
		T_{25}	**-0.083**	**-0.292; 0.126**	
		P_{25}	**0.281**	**0.180; 0.383**	*****
		T_{25} × Site (food-restricted)	**-0.330**	**-0.533; -0.127**	*****
		Site (food-restricted)	-0.252	-0.434; -0.071	*
30 days	$\sigma^2_{Year} = 0.110$	Intercept	2.298	1.813; 2.782	*
		Julian day	-0.037	-0.132; 0.057	
		T_{30}	**-0.113**	**-0.356; 0.130**	
		P_{30}	**0.242**	**0.139; 0.345**	*****
		T_{30} × Site (food-restricted)	**-0.253**	**-0.483; -0.023**	*****
		Site (food-restricted)	-0.280	-0.467; -0.092	*

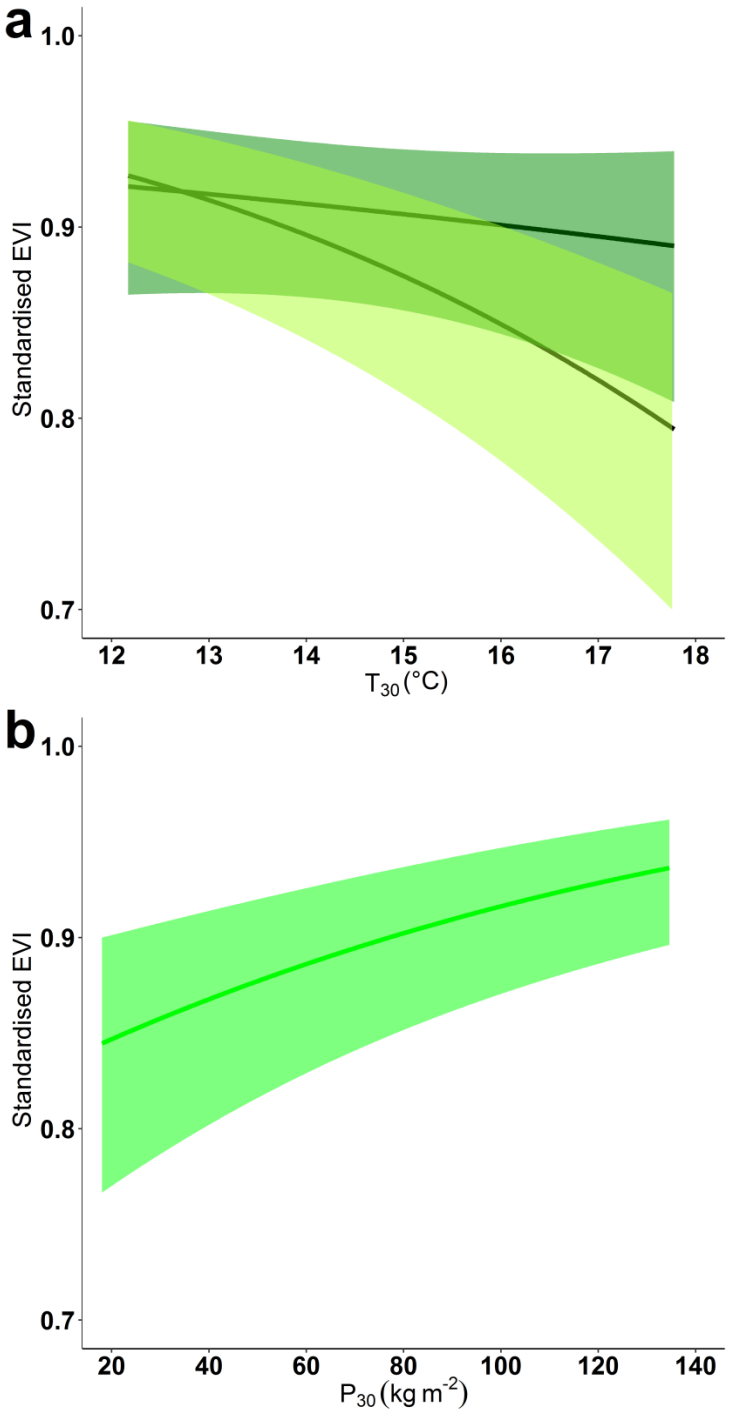

Figure S1. Effects of (a) mean temperature (T_{30}) and (b) total amount of rainfall (P_{30}) accumulated over 30 days prior to focal observation day on the standardized EVI. In (a), the interactive effect of T_{30} and study site is shown (light green: food-restricted site; dark green: food-rich site). Lines and shading: values predicted while averaging the effects of other confounding variables and 95% confidence intervals.

Appendix 4. Analysis of the direct effects of temperature on aggression indices

Table S7. Result of the model selection conducted to investigate the direct effects of temperature (T) on the *pro capite* aggression rate of chamois. The top-ranked, non-nested models within ΔAICc<2 are shown, with relevant K, AICc, ΔAICc and standardized weight. All models evaluated also included the chamois group identity as random intercept.

Intercept	T	Site	Time	Time^2	Julian day	T × Site	K	AICc	ΔAICc	Weight
X			X	X			6	1839.2	0	0.69
X			X				5	1840.8	1.6	0.31

Table S8. Result of the model selection conducted to investigate the direct effects of temperature (T) on the probability of delivering a more aggressive behaviour pattern by chamois during feeding contests. The top-ranked, non-nested models within ΔAICc<2 are shown, with relevant K, AICc, ΔAICc and standardized weight. All models evaluated also included the chamois group identity as random intercept.

Intercept	T	Site	Time	Time^2	Julian day	Opponent's relative age	Sender's age class	Contest type	T × Site	P × Site	K	AICc	ΔAICc	Weight
X					X	X		X			6	819.5	0	1

Appendix 5. Analysis of the proximate effect of vegetation productivity on aggression indices

Table S9. Result of the model selection conducted to investigate the effect of vegetation productivity (standardized EVI index) on the *pro capite* aggression rate of chamois. The top-ranked, non-nested models within ΔAICc<2 are shown, with relevant K, AICc, ΔAICc and standardized weight. All models evaluated also included the chamois group identity as random intercept.

Intercept	EVI	Site	Time	Time^2	Julian day	EVI × Site	K	AICc	ΔAICc	Weight
X	X		X	X	X		8	1833.3	0	0.46
X	X		X	X			7	1834.0	0.70	0.33
X	X		X		X		7	1834.9	1.62	0.21

Table S10. Result of the model selection conducted to investigate the effect of vegetation productivity (standardized EVI index) on the probability of delivering a more aggressive behaviour pattern by chamois during feeding contests. The top-ranked, non-nested models within ΔAICc<2 are shown, with relevant K, AICc, ΔAICc and standardized weight. All models evaluated also included the chamois group identity as random intercept.

Intercept	EVI	Site	Time	Time^2	Julian day	Opponent's relative age	Sender's age class	Contest type	T × EVI	K	AICc	ΔAICc	Weight
X	X				X	X		X		7	817.5	0	1

Table S11. Parameters estimated from the best GLMM predicting (a) the *pro capite* aggression rate of chamois at feeding and (b) the probability of delivering a more aggressive behaviour pattern by chamois during feeding contests, in relation to vegetation productivity: variance of random intercepts (σ^2), predictors' coefficient estimates (β) and their 95% confidence intervals (CIs). An asterisk marks coefficients whose CIs do not include '0'. Effects of vegetation productivity on aggression indices are bolded. For measurement units of explanatory variables, see main text.

Response variable	**Random intercept**	**Predictor**	**β coefficient**	**95% CI**	
a. Pro capite intra-group aggression rate	$\sigma^2_{GroupID} = 0.303$	Intercept	-3.275	-3.452; -3.098	*
		EVI	**-0.303**	**-0.488; -0.118**	*****
		Time of day	0.232	0.054; 0.410	*
		Time of day^2	0.148	-0.004; 0.299	
		Julian day	-0.161	-0.353; 0.031	
b. Aggression intensity	$\sigma^2_{GroupID} = 0.478$	Intercept	2.188	1.789; 2.588	*
		EVI	**-0.346**	**-0.683; -0.009**	*****
		Julian day	0.334	0.021; 0.646	*
		Opponent's relative age (same)	0.508	0.053; 0.963	*
		Opponent's relative age (older)	-0.362	-0.907; 0.184	
		Contest type (escalated)	-0.806	-1.191; -0.421	*

Appendix 6. Model validation

Using the R package *DHARMa* (Hartig 2022), we inspected the residuals of each best model to identify potential model misspecification. As interpreting conventional residuals for GL(M)Ms is often problematic (see Hartig 2022), this package uses a simulation-based approach to create scaled (quantile) residuals for GL(M)Ms, which are standardized to values between 0 and 1, and can be interpreted more easily. For each best model, qq-plot of the simulated residuals was inspected to check for their uniformity. A nonparametric dispersion test (two-tailed, α=0.01) was also performed by comparing the standard deviation of the fitted residuals against that of the simulated ones, in order to test for potential over- or underdispersion.

For the best models predicting the *pro capite* aggression rate and standardized EVI, the goodness of fit was assessed by comparing the observed values to those predicted by considering model parameters while adding randomly simulated errors specifically generated for each model and based on their assumed error distribution. Thus, for the best models predicting the *pro capite* aggression rate and standardized EVI, 10,000 distributions of the predicted values were generated assuming respectively Tweedie or beta errors, using the R functions *rTweedie* and *rbeta*. Then, the distribution of observed values was compared against each distribution of predicted values by using a Kolmogorov-Smirnov (KS) test (two-tailed; α=0.05; H_0: the two distributions do not differ from each other), thus performing 10,000 KS tests through the R function *ks.test*. For the best model predicting aggression intensity, given that the outcome of this model is binary, the goodness of fit was evaluated by building the ROC curve and calculating relevant AUC (through the R package *pROC*; Robin et al. 2011), as recommended for logistic models. Using a 0.5 cut-off, we also calculated model accuracy (i.e., the sum of the number of observations correctly predicted as 0 and the number of observations correctly predicted as 1, divided by the total number of observations).

For every model run (Appendices 1-3), the dispersion test was not significant and misspecifications were not detected (Figure S2). For the best models predicting the *pro capite* aggression rate (Appendix

1) and standardized EVI (Appendix 3), respectively 99.5% and 72.8% p-values (30 days), 99.7% and 73.4% p-values (25 days), 99.7% and 89.8% p-values (20 days), and 99.9% and 92.3% p-values (15 days) of the KS tests were greater than 0.05, meaning that in most cases the distribution of the predicted values reflected that of the observed ones (Figure S3a,c), confirming the good fit of these models. For the best models predicting aggression intensity (Appendix 2), accuracy was 83.7% and AUC=0.78 (30 days), 83.7% and AUC=0.78 (25 days), 83.7% and AUC=0.78 (20 days), and 83.5% and AUC=0.78 (15 days) (Figure S3b), confirming the good fit of these models. The same results occurred for model predicting the *pro capite* aggression rate and aggression intensity in relation to EVI (Appendix 5), showing no misspecification and, respectively, having 98% p-values greater than 0.05 (Figure S4a), and 83.5% accuracy and AUC=0.78 (Figure S4b).

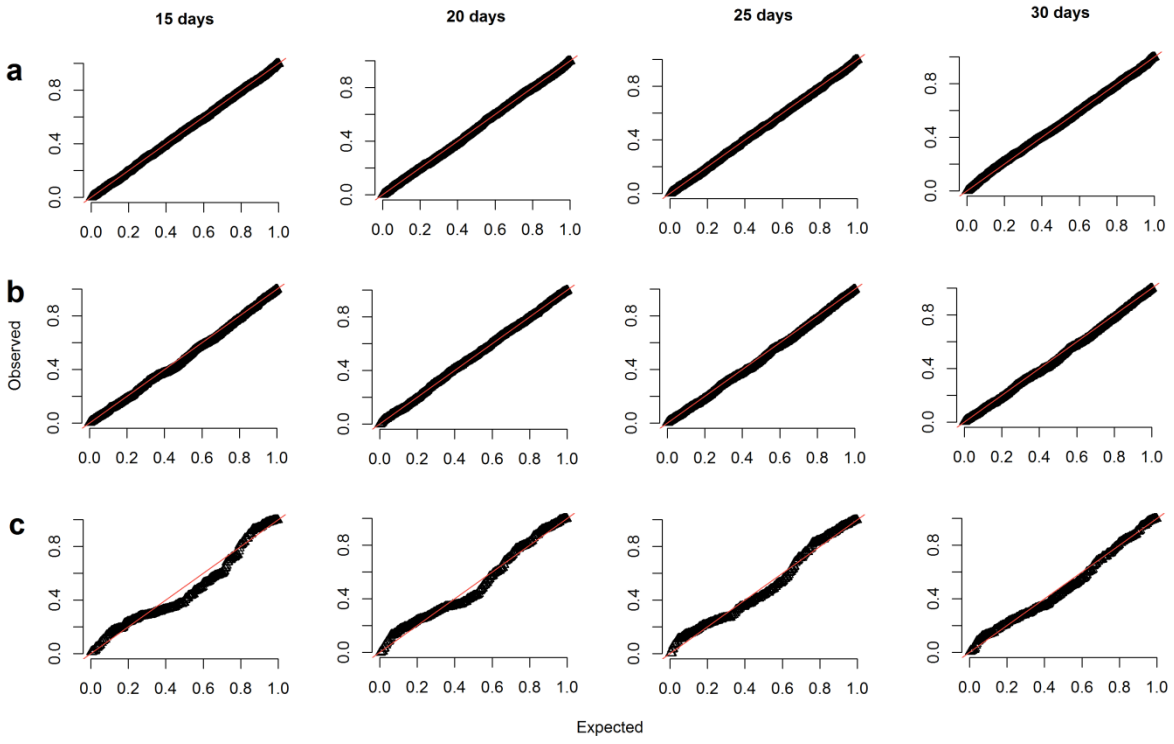

Figure S2. For each best model run at each time window (a: *pro capite* aggression rate, b: aggression intensity, c: standardized EVI), a qq-plot of the scaled residuals showing overall deviations from the expected (red line) distribution is depicted.

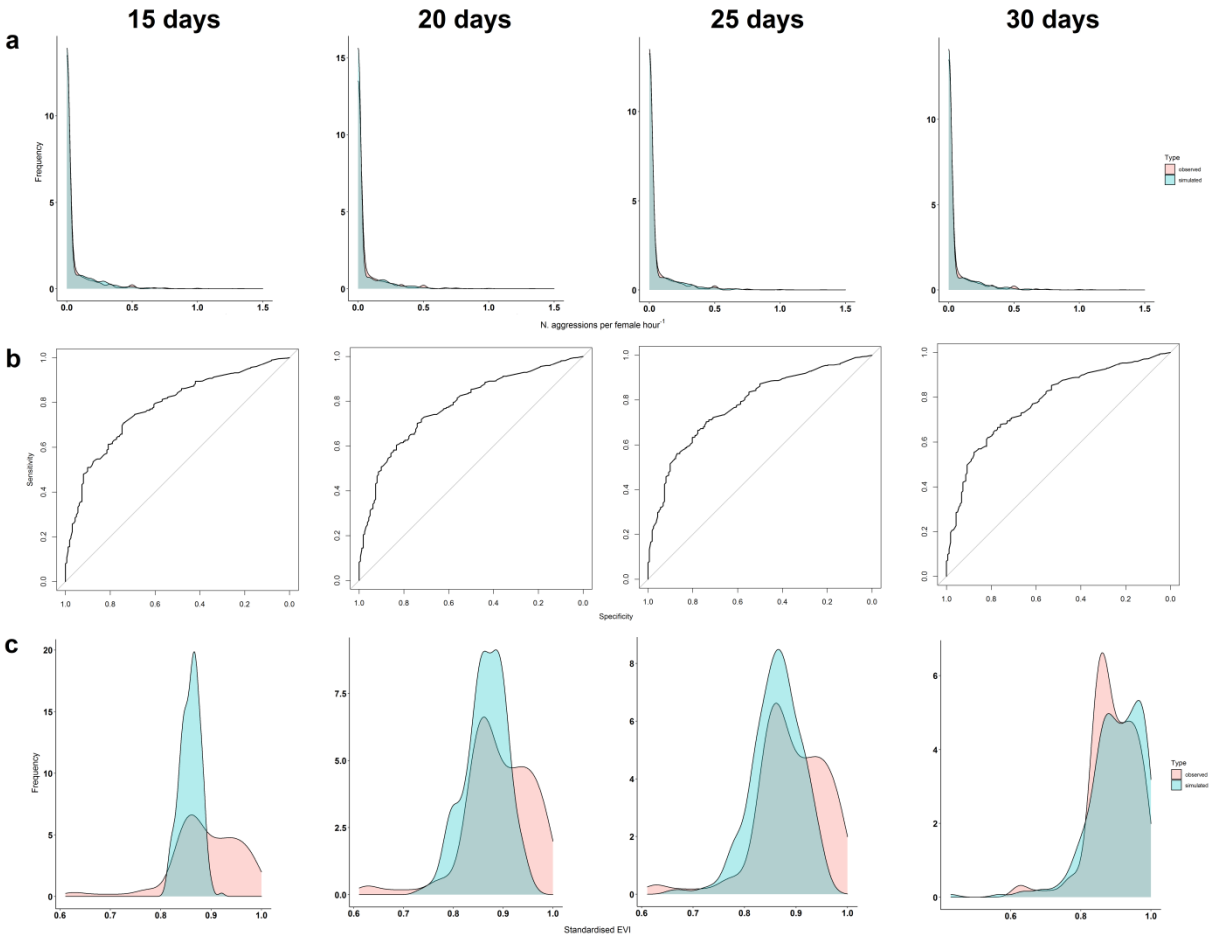

Figure S3. For each best model run at each time window (a: *pro capite* aggression rate, b: aggression intensity, c: standardized EVI), goodness of fit is shown. In (a) and (c), the figure shows the (kernel) frequency distributions of both the observed values and the values predicted by the model using one of the 10,000 simulated error distributions. In (b), the figure shows the ROC curve.

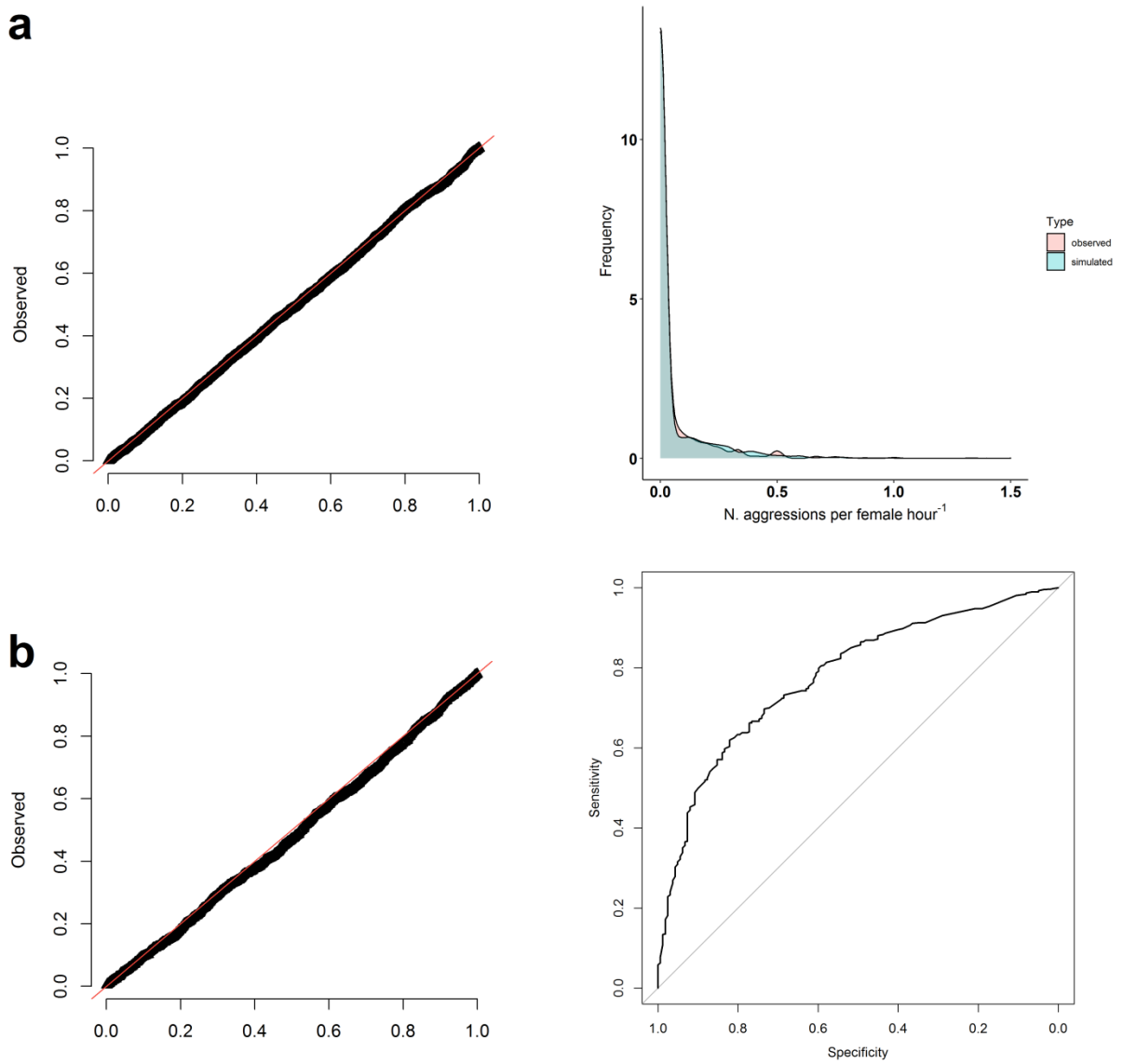

Figure S4. For each best model predicting (a) the *pro capite* aggression rate and (b) aggression intensity in relation to EVI, a qq-plot of the scaled residuals showing overall deviations from the expected (red line) distribution is depicted, together with goodness of fit (a: kernel frequency distributions of both the observed values and the values predicted by the model using one of the 10,000 simulated error distributions; b: ROC curve).

Appendix 7. Projection of future accumulated temperature in our study area

Historical weather data in our study area are available from 1990 onwards. We considered the 30 days-cumulative temperature (T_{30}) and precipitation (P_{30}) recorded in our study area in the period 1990-2020 to predict trajectories of accumulated temperature and rainfall for the next 60 years, up to 2080. We fixed the date at the 1st August, to simulate aggression indices of chamois at the median date of the study period, and to allow validating our local projections with those forecasted by global scenarios, which are available at the monthly scale (see Appendix 8). Whereas T_{30} showed a significantly linear increase in our study area, in the period 1990-2020 (OSL regression; Table S12 and Fig. 2a in main text), P_{30} did not vary (Table S12). Hence, we only projected trajectories of future T_{30}. Because there have been linear/exponential increases in global temperatures during the last decades (Hegerl et al. 2018), our projection assumed no major variation of the trend of temperature increase in the next few decades, up to 2080. From 2021 to 2080, 10000 trajectories of T_{30} were simulated according to the following linear model:

$$T_{30,t,i} = \alpha + \beta t + \varepsilon_{t,i},\ t = 2021,\ldots,2080,\ i = 1,\ldots,10000,$$

where $T_{30,t,i}$ denotes the mean spring temperature of the i-th trajectory for the year t, α and β were the OLS estimates (Table S12), and $\varepsilon_{t,i}$ was the error term assumed to be a normal random variable with 0 expectation and variance σ^2 estimated by the residual variance of the OLS regression (Table S12). As the OLS regression of T_{30} in the period 1990-2020 did not show autocorrelated residuals (Durbin-Watson test; $p = 0.156$), we did not assume them in our simulations.

Table S12. Parameters estimated by OLS regressions conducted to determine the trends of T_{30} and P_{30} through years, in the period 1990-2020.

	Intercept α	**Regression Coefficient β (SE)**	**p-value**	**Residual variance σ^2**
T_{30}	-80.37	0.047 (0.023)	0.049	1.20
P_{30}	-988.77	0.521 (0.686)	0.460	1005.90

Appendix 8. Concordance of locally-projected temperature with CMIP6 global scenarios

Because temperatures predicted by global circulation models (GCMs) are not comparable, in absolute value, to those recorded at weather stations (which we used to build our local projections), we compared the future *change* in temperature (ΔT, in °C) projected by our simulations to that projected in our study area using GCMs and four "Shared Socioeconomic Pathways" (SSPs; SSP1-2.6, SSP2-4.5, SSP4-6.0, and SSP5-8.5), corresponding to four different scenarios of climate policy encompassing the likely range of future radiative forcing.

We downloaded data from Worldclim 2.1 (Fick & Hijmans 2017), considering GCMs with available projections for all the four SSPs (i.e., 21 GCMs; Table S13), totalling 84 different scenarios. As our projections of accumulated temperature are based on the mean temperatures within 30 days prior to the 1st August, thus reflecting the mean temperature of July, we had to use the monthly data of July. We used data at the spatial resolution of 2.5 min (approximately corresponding to cells of size 3.5 × 4.5 km), i.e. the minimum resolution available to match these future projections with historical monthly Worldclim data. Future projections of monthly temperatures are available for 2030 (average for 2021-2040) and 2070 (average for 2061-2080), while the monthly reference data used was the year 1990, corresponding to our first observed year of data. Therefore, we were able to compare temperature changes forecasted by CMIP6 projections with ours, in the periods 1990-2030 and 2030-2070. To make comparisons, we used the ensemble of 84 scenarios by considering the average of all the predicted outcomes, as customary when selecting climate models (Seager et al. 2007).

Comparison shows that our projected increase in temperature is consistent with the mean increase projected by the ensemble of 84 CMIP6 scenarios (Table S14). In particular, our projections of temperature used to simulate the future aggression rate of chamois are robust, as being included in the 95% confidence interval of temperature changes based on four SSPs reflecting the possible range of future radiative forcing (Figure S5).

Table S13. Details of Global Circulation Models (GCMs) used for the comparison between our temperature change projections and those of CMIP6 scenarios.

GCM	Resolution (°lon × °lat)	Reference
ACCESS-ESM1-5	1.9 × 1.2	Law et al. 2017
BCC-CSM2-MR	1.1 × 1.1	Wu et al. 2019
CanESM5	2.8 × 2.8	Swart et al. 2019
CanESM5-CanOE	2.8 × 2.8	Swart et al. 2019
CMCC-ESM2	0.9 × 1.2	Lovato et al. 2022
CNRM-CM6-1	1.4 × 1.4	Voldoire et al. 2019
CNRM-CM6-1-HR	0.5 × 0.5	Voldoire et al. 2019
CNRM-ESM2-1	1.4 × 1.4	Séférian et al. 2019
EC-Earth3-Veg	0.7 × 0.7	Wyser et al. 2020, Döscher et al. 2022
EC-Earth3-Veg-LR	0.7 × 0.7	Wyser et al. 2020; Döscher et al. 2022
GISS-E2-1-G	1.2 × 1.0	Rind et al. 2020
GISS-E2-1-H	1.0 × 1.0	Rind et al. 2020
INM-CM4-8	2.0 × 1.5	Volodin et al. 2018
INM-CM5-0	2.0 × 1.5	Volodin et al. 2018
IPSL-CM6A-LR	2.5 × 1.3	Lurton et al. 2020
MIROC-ES2L	2.8 × 2.8	Hajima et al. 2020
MIROC6	1.4 × 1.4	Tatebe et al. 2019
MPI-ESM1-2-HR	0.9 × 0.9	Gutjahr et al. 2019
MPI-ESM1-2-LR	1.9 × 1.9	Mauritsen et al. 2019
MRI-ESM2-0	1.1 × 1.1	Yukimoto et al. 2019
UKESM1-0-LL	1.9 × 1.3	Sellar et al. 2019

Table S14. Changes in temperature, ΔT, in the two periods (CMIP6 scenarios: mean; our projection: difference between 50th percentile and the observed value, for 1990-2030, or 50th percentile, for 2030-2070, of the previous time period). Brackets report variability of ΔT (CMIP6 scenarios: 95% confidence limits; our projection: difference between both 75th and 25th percentile with the observed value, for 1999-2030, or with 50th percentile of the previous time period, for 2030-2070, to reflect 50% trajectories used to simulate aggression rate of chamois).

Projection	**$\Delta T_{1990\text{-}2030}$ (°C)**	**$\Delta T_{2030\text{-}2070}$ (°C)**
SSP 126 (n=21)	2.30 [1.77; 2.84]	0.65 [0.41; 0.90]
SSP 245 (n=21)	2.32 [1.82; 2.83]	1.73 [1.40; 2.07]
SSP 370 (n=21)	2.28 [1.79; 2.77]	2.58 [2.29; 2.87]
SSP 585 (n=21)	2.44 [1.91; 2.98]	3.37 [3.00; 3.74]
Ensemble (n=84)	**2.34 [1.83; 2.84]**	**2.08 [1.55; 2.61]**
Our projection	**1.95 [1.21; 2.69]**	**1.91 [1.17; 2.66]**

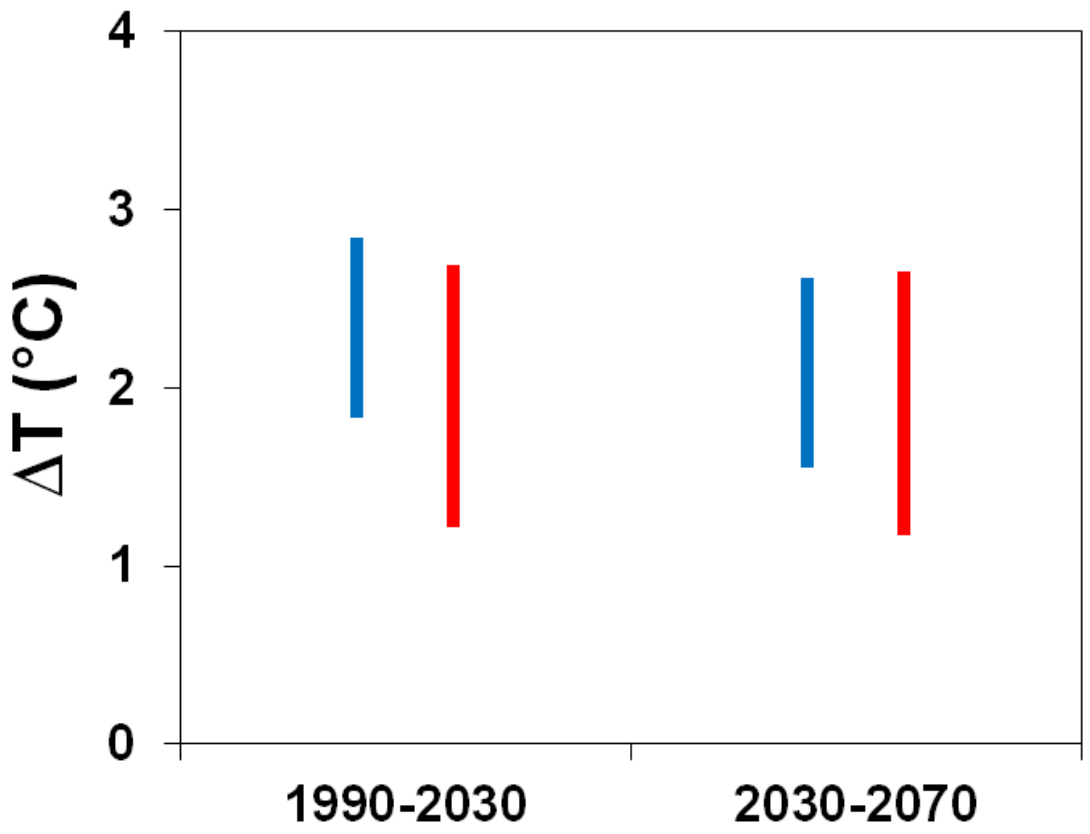

Figure S4. Variability of the projected changes in temperature, ΔT, in the two periods (CMIP6 scenarios: 95% confidence limits; our projection: difference between both 75th and 25th percentile with the observed value, for 1999-2030, or with 50th percentile of the previous time period, for 2030-2070, to reflect 50% trajectories used to simulate aggression rate of chamois). Blue bars: CMIP6 scenarios; red bars: our projection.

Appendix 9. Future variation in chamois aggression rate

Table S15. Simulated *pro capite* aggression rate of chamois in the period 2021-2080, showing the mean annual number of aggressions per female hour^{-1} and relevant percentage of variation compared to the year 2021, at each daytime period (-5, 0 and 5 hours from noon).

	-5 h		0 h		5 h	
Year	**Aggression rate**	**% variation**	**Aggression rate**	**% variation**	**Aggression rate**	**% variation**
2021	0.6048	-	0.6167	-	1.4118	-
2022	0.5896	-2.51%	0.6031	-2.20%	1.4294	1.24%
2023	0.5764	-4.70%	0.6377	3.41%	1.3738	-2.70%
2024	0.5570	-7.91%	0.6352	3.02%	1.4655	3.80%
2025	0.5897	-2.50%	0.6258	1.48%	1.4605	3.45%
2026	0.6056	0.13%	0.6738	9.26%	1.4296	1.26%
2027	0.6219	2.82%	0.6447	4.54%	1.4958	5.95%
2028	0.6329	4.65%	0.6700	8.64%	1.4682	3.99%
2029	0.6300	4.17%	0.6951	12.72%	1.5285	8.27%
2030	0.6062	0.23%	0.6536	5.99%	1.5037	6.51%
2031	0.6070	0.36%	0.6991	13.37%	1.5385	8.97%
2032	0.6244	3.24%	0.6877	11.52%	1.5220	7.81%
2033	0.5903	-2.40%	0.7078	14.78%	1.5343	8.67%
2034	0.6519	7.79%	0.6836	10.86%	1.5530	10.00%
2035	0.6601	9.14%	0.6928	12.36%	1.5836	12.17%
2036	0.6457	6.77%	0.7023	13.88%	1.6394	16.12%
2037	0.6481	7.15%	0.6997	13.46%	1.5725	11.38%
2038	0.6515	7.72%	0.7216	17.03%	1.6317	15.57%
2039	0.6496	7.40%	0.7210	16.91%	1.6324	15.62%
2040	0.6589	8.94%	0.7387	19.79%	1.5902	12.64%
2041	0.6680	10.45%	0.7472	21.17%	1.6210	14.81%
2042	0.6842	13.12%	0.7564	22.67%	1.6427	16.35%
2043	0.6909	14.23%	0.7061	14.50%	1.6379	16.01%
2044	0.6731	11.29%	0.7255	17.65%	1.6656	17.97%
2045	0.6512	7.68%	0.7159	16.09%	1.6399	16.15%
2046	0.6894	13.98%	0.7168	16.25%	1.6472	16.67%
2047	0.6906	14.18%	0.7486	21.39%	1.6929	19.91%
2048	0.6713	10.98%	0.7355	19.28%	1.6964	20.15%
2049	0.7037	16.34%	0.7815	26.73%	1.6984	20.30%
2050	0.7186	18.81%	0.7681	24.55%	1.7896	26.76%
2051	0.7170	18.55%	0.7643	23.94%	1.7555	24.34%
2052	0.7151	18.23%	0.7859	27.45%	1.7397	23.22%
2053	0.7085	17.15%	0.7676	24.48%	1.7828	26.28%
2054	0.7481	23.70%	0.7758	25.82%	1.7442	23.54%

2055	0.6906	14.18%	0.7728	25.32%	1.7582	24.53%
2056	0.7326	21.13%	0.8175	32.57%	1.7776	25.90%
2057	0.7631	26.17%	0.8138	31.97%	1.8464	30.78%
2058	0.7558	24.96%	0.8059	30.69%	1.8713	32.54%
2059	0.7661	26.66%	0.8271	34.12%	1.8412	30.41%
2060	0.7660	26.66%	0.8026	30.15%	1.8189	28.83%
2061	0.7821	29.32%	0.8173	32.54%	1.8245	29.23%
2062	0.7595	25.58%	0.8502	37.87%	1.8559	31.45%
2063	0.7783	28.69%	0.8585	39.23%	1.8694	32.41%
2064	0.7808	29.10%	0.8635	40.03%	1.9122	35.44%
2065	0.7890	30.45%	0.8894	44.23%	1.8651	32.10%
2066	0.8037	32.89%	0.8546	38.59%	1.8517	31.16%
2067	0.7863	30.01%	0.8157	32.27%	1.8299	29.61%
2068	0.7857	29.91%	0.8707	41.20%	1.9679	39.39%
2069	0.7661	26.66%	0.8492	37.71%	1.9388	37.32%
2070	0.8060	33.26%	0.8385	35.97%	1.9794	40.20%
2071	0.8045	33.02%	0.8879	43.99%	2.0551	45.56%
2072	0.8319	37.55%	0.8840	43.36%	2.0092	42.31%
2073	0.8201	35.60%	0.9113	47.79%	2.0247	43.41%
2074	0.8095	33.85%	0.8944	45.04%	2.0284	43.67%
2075	0.8396	38.82%	0.8988	45.75%	2.0537	45.46%
2076	0.8379	38.54%	0.9056	46.86%	2.0816	47.44%
2077	0.8339	37.88%	0.9060	46.92%	2.0648	46.24%
2078	0.8621	42.53%	0.9306	50.92%	2.0254	43.46%
2079	0.8585	41.94%	0.9571	55.21%	2.1655	53.38%
2080	0.8694	43.75%	0.9597	55.63%	2.1393	51.52%

References

Döscher R., Acosta M., Alessandri A., Anthoni P., Arsouze T., Bergman T., Bernardello R., Boussetta S., Caron L.-P., Carver G., Castrillo M., Catalano F., Cvijanovic I., Davini P., Dekker E., Doblas-Reyes F.J., Docquier D., Echevarria P., Fladrich U., Fuentes-Franco R., Gröger M., von Hardenberg J., Hieronymus J., Pasha Karami M., Keskinen J.-P., Koenigk T., Makkonen R., Massonnet F., Ménégoz M., Miller P.A., Moreno-Chamarro E., Nieradzik L., van Noije T., Nolan P., O'Donnell D., Ollinaho P., van den Oord G., Ortega P., Tintó Prims O., Ramos A., Reerink T., Rousset C., Ruprich-Robert Y., Le Sager P., Schmith T., Schrödner R., Serva F., Sicardi V., Sloth Madsen M., Smith B., Tian T., Tourigny E., Uotila P., Vancoppenolle M., Wang S., Wårlind D., Willén U., Wyser K., Yang S., Yepes-Arbós X., & Zhang Q. (2022). The EC-Earth3 Earth system model for the Coupled Model Intercomparison Project 6. *Geoscientific Model Development*, 15, 2973-3020.

Fick S.E., & Hijmans R.J. (2017). WorldClim 2: new 1-km spatial resolution climate surfaces for global land areas. *International Journal of Climatology*, 37, 4302-4315.

Gutjahr O., Putrasahan D., Lohmann K., Jungclaus J.H., von Storch J.-S., Brüggemann N., Haak H., & Stössel A. (2019). Max Planck Institute Earth System Model (MPI-ESM1.2) for the High-Resolution Model Intercomparison Project (HighResMIP). *Geoscientific Model Development*, 12, 3241-3281.

Hajima T., Watanabe M., Yamamoto A., Tatebe H., Noguchi M.A., Abe M., Ohgaito R., Ito A., Yamazaki D., Okajima H., Ito A., Takata K., Ogochi K., Watanabe S., & Kawamiya M. (2020). Description of the MIROC-ES2L Earth system model and evaluation of its climate-biogeochemical processes and feedbacks. *Geoscientific Model Development*, 13, 2197-2244.

Hartig F. (2022). *DHARMa: residual diagnostics for hierarchical (multi-level/mixed) regression models*. R package version 0.4.6. https://CRAN.R-project.org/package=DHARMa

Hegerl G.C., Brönnimann S., Schurer A., & Cowan T. (2018). The early 20th century warming: anomalies, causes, and consequences. *WIREs Climate Change*, 9, e522.

Law R.M., Ziehn T., Matear R.J., Lenton A., Chamberlain M.A., Stevens L.E., Wang Y.-P., Srbinovsky J., Bi D., Yan H., & Vohralik P.F. (2017). The carbon cycle in the Australian Community Climate and Earth System Simulator (ACCESS-ESM1)—Part 1: model description and pre-industrial simulation. *Geoscientific Model Development*, 10, 2567-2590.

Lovato T., Peano D., Butenschön M., Materia S., Iovino D., Scoccimarro E., Fogli P.G., Cherchi A., Bellucci A., Gualdi S., Masina S., & Navarra A. (2022). CMIP6 simulations with the CMCC Earth System Model (CMCC-ESM2). *Journal of Advances in Modeling Earth Systems*, 14, e2021MS002814.

Lurton T., Balkanski Y., Bastrikov V., Bekki S., Bopp L., Braconnot P., Brockmann P., Cadule P., Contoux C., Cozic A., & Cugnet D. (2020). Implementation of the CMIP6 Forcing Data in the IPSL CM6A LR Model. *Journal of Advances in Modeling. Earth Systems*, 12, e2019MS001940.

Mauritsen T., Bader J., Becker T., Behrens J., Bittner M., Brokopf R., Brovkin V., Claussen M., Crueger T., Esch M., Fast I., Fiedler S., Fläschner D., Gayler V., Giorgetta M., Goll D.S., Haak H., Hagemann S., Hedemann C., Hohenegger C., Ilyina T., Jahns T., Jimenéz-de-la-Cuesta D., Jungclaus J., Kleinen T., Kloster S., Kracher D., Kinne S., Kleberg D., Lasslop G., Kornblueh L., Marotzke J., Matei D., Meraner K., Mikolajewicz U., Modali K., Möbis B., Müller W.A., Nabel J.E.M.S., Nam C.C.W., Notz D., Nyawira S.-S., Paulsen H., Peters K., Pincus R., Pohlmann H., Pongratz J., Popp M., Raddatz T.J., Rast S., Redler R., Reick C.H., Rohrschneider T., Schemann V., Schmidt H., Schnur R., Schulzweida U., Six K.D., Stein L., Stemmler I., Stevens B., von Storch J.-S., Tian F., Voigt A., Vrese P., Wieners K.-H., Wilkenskjeld S., Winkler A., & Roeckner E. (2019). Developments in the MPI-M

Earth System Model version 1.2 (MPI-ESM1.2) and its response to increasing CO2. *Journal of Advances in Modeling Earth Systems*, 11, 998-1038.

Rind D., Orbe C., Jonas J., Nazarenko L., Zhou T., Kelley M., Lacis A., Shindell D., Faluvegi G., Romanou A., Russell G., Tausnev N., Bauer M., & Schmidt G. (2020). GISSModel E2.2: A Climate Model Optimized for the Middle Atmosphere – Model Structure, Climatology, Variability, and Climate Sensitivity. *Journal of Geophysical Research: Atmosphere*, 125, e2019JD032204.

Robin X., Turck N., Hainard A., Tiberti N., Lisacek F., Sanchez J.C., & Müller M. (2011). pROC: an open-source package for R and S+ to analyze and compare ROC curves. *BMC Bioinformatics*, 12, 77.

Seager R., Ting M., Held I., Kushnir Y., Lu J., Vecchi G., Huang H.-P., Harnik N., Leetmaa A., & Lau N.-C. (2007). Model projections of an imminent transition to a more arid climate in southwestern North America. *Science*, 316, 1181-1184.

Séférian R., Nabat P., Michou M., Saint-Martin D., Voldoire A., Colin J., Decharme B., Delire C., Berthet S., Chevallier M., Sénési S., Franchisteguy L., Vial J., Mallet M., Joetzjer E., Geoffroy O., Guérémy J.-F., Moine M.-P., Msadek R., Ribes A., Rocher M., Roehrig R., Salas-y-Mélia D., Sanchez E., Terray L., Valcke S., Waldman R., Aumont O., Bopp L., Deshayes J., Éthé C., & Madec G. (2019). Evaluation of CNRM Earth-System model, CNRMESM2-1: role of Earth system processes in present-day and future climate. *Journal of Advances in Modeling Earth Systems*, 11, 4182-4227.

Sellar A., Jones C., Mulcahy J., Tang Y., Yool A., Wiltshire A., O'Connor F., Stringer M., Hill R., Palmieri J., Woodward S., Mora L., Kuhlbrodt T., Rumbold S., Kelley D., Ellis R., Johnson C., Walton J., Abraham N., Andrews M., Andrews T., Archibald A., Berthou S., Burke E., Blockley E., Carslaw K., Dalvi M., Edwards J., Folberth G., Gedney N., Griffiths P., Harper A., Hendry M., Hewitt A., Johnson B., Jones A., Jones C., Keeble J., Liddicoat S., Morgenstern O., Parker R., Predoi V.,

Robertson E., Siahaan A., Smith R., Swaminathan R., Woodhouse M., Zeng G., & Zerroukat M. (2019). UKESM1: description and evaluation of the UK Earth system model. *Journal of Advances in Modeling Earth Systems*, 11, 4513-4558.

Swart N.C., Cole J.N.S., Kharin V.V., Lazare M., Scinocca J.F., Gillett N.P., Anstey J., Arora V., Christian J.R., Hanna S., Jiao Y., Lee W.G., Majaess F., Saenko O.A., Seiler C., Seinen C., Shao A., Sigmond M., Solheim L., von Salzen K., Yang D., & Winter B. (2019). The Canadian Earth System Model version 5 (CanESM5.0.3). *Geoscientific Model Development*, 12, 4823-4873.

Tatebe H., Ogura T., Nitta T., Komuro Y., Ogochi K., Takemura T., Sudo K., Sekiguchi M., Abe M., Saito F., Chikira M., Watanabe S., Mori M., Hirota N., Kawatani Y., Mochizuki T., Yoshimura K., Takata K., O'ishi R., Yamazaki D., Suzuki T., Kurogi M., Kataoka T., Watanabe M., & Kimoto M. (2019). Description and basic evaluation of simulated mean state, internal variability, and climate sensitivity in MIROC6. *Geoscientific Model Development*, 12, 2727-2765.

Voldoire A., Saint-Martin D., Sénési S., Decharme B., Alias A., Chevallier M., Colin J., Guérémy J.-F., Michou M., Moine M.-P., Nabat P., Roehrig R., Salas y Mélia D., Séférian R., Valcke S., Beau I., Belamari S., Berthet S., Cassou C., Cattiaux J., Deshayes J., Douville H., Ethé C., Franchistéguy L., Geoffroy O., Lévy C., Madec G., Meurdesoif Y., Msadek R., Ribes A., Sanchez-Gomez E., Terray L., & Waldman R. (2019). Evaluation of CMIP6 DECK experiments with CNRM-CM6-1. *Journal in Advances of Modeling Earth Systems*, 11, 2177-2213.

Volodin E.M., Mortikov E.V., Kostrykin S.V., Galin V.Y., Lykossov V.N., Gritsun A.S., Diansky N.A., Gusev A.V., Iakovlev N.G., Shestakova A.A., & Emelina S.V. (2018). Simulation of the modern climate using the INM-CM48 climate model. *Russian Journal of Numerical Analysis and Mathematical Modelling*, 33, 367-374.

Wu T., Lu Y., Fang Y., Xin X., Li L., Li W., Jie W., Zhang J., Liu Y., Zhang L., Zhang F., Zhang Y., Wu F., Li J., Chu M., Wang Z., Shi X., Liu X., Wei M., Huang A., Zhang Y., & Liu X. (2019). The Beijing Climate Center Climate System Model (BCC-CSM): the main progress from CMIP5 to CMIP6. *Geoscientific Model Development*, 12, 1573-1600.

Wyser K., van Noije T., Yang S., von Hardenberg J., O'Donnell D., & Döscher R. (2020). On the increased climate sensitivity in the EC-Earth model from CMIP5 to CMIP6. *Geoscientific Model Development*, 13, 3465-3474.

Yukimoto S., Kawai H., Koshiro T., Oshima N., Yoshida K., Urakawa S., Tsujino H., Deushi M., Tanaka T., Hosaka M., Yabu S., Yoshimura H., Shindo E., Mizuta R., Obata A., Adachi Y., & Ishii M. (2019). The Meteorological Research Institute Earth System Model version 2.0, MRI-ESM2.0: description and basic evaluation of the physical component. *Journal of the Meteorological Society of Japan - Ser. II*, 97, 931-965.